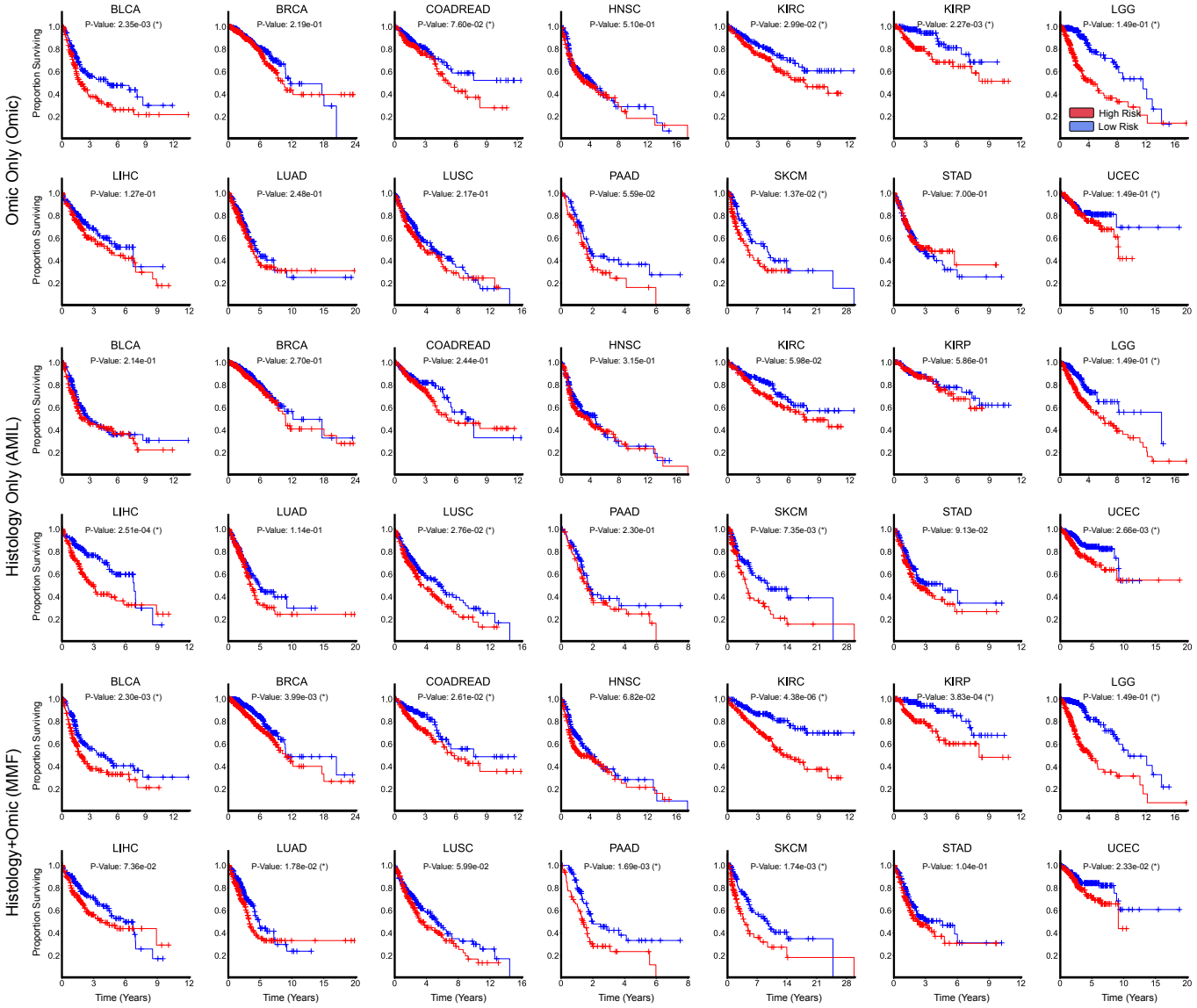

Figure S1: Kaplan-Meier comparative analysis of SNN, AMIL, and MMF. Related to Figure 2. Kaplan-Meier comparative analysis of SNN, AMIL, and MMF of patient stratification of low- and high-risk patients across all 14 cancer types. low- and high-risks are defined by the median 50% percentile of risk predictions. Logrank test was used to test for statistical significance in survival distributions between low- and high-risk patients (with * marked if P-Value < 0.05). For all model types and cancer types, out-of-sample risk predictions in the validation folds were pooled to show overall survival distribution on the entire cohort.

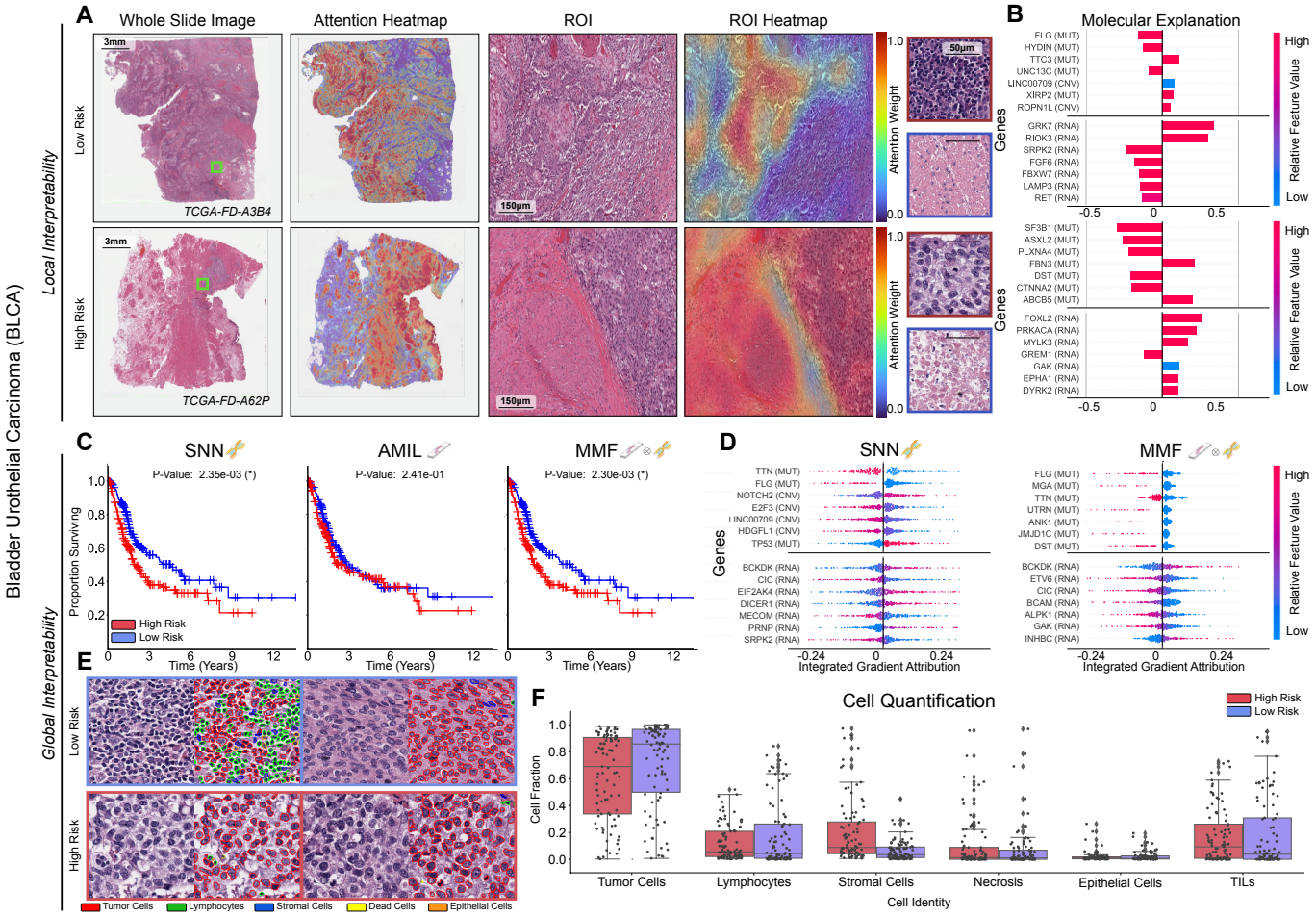

Figure S2: Quantitative performance, local model explanation, and global interpretability pooled analyses of PORPOISE on BLCA. Related to Figure 3, 4, 5, and 6. A. WSIs, associated attention heatmaps, ROIs, ROI heatmaps, and selected high attention patches from example low-risk (top) and high-risk (bottom) cases. In BLCA (n=358), high attention for low-risk cases (n=90) tends to focus on aggregates of lymphocytes, thick tumor papillae, and muscularis, while in high-risk cases (n=93), high attention focuses on sheet-like and solid tumor growth, muscularis, and areas of necrosis. **B.** Local gene attributions for the corresponding low-risk (top) and high-risk (bottom) cases. **C.** Kaplan–Meier curves for omics-only (left, "SNN"), histology-only (center, "AMIL") and multimodal fusion (right, "MMF"), showing improved patient stratification over AMIL and long-surviving patients in SNN. **D.** Global gene attributions across patient cohorts according to unimodal interpretability (left, "SNN"), and multimodal interpretability (right, "MMF"). **E.** High attention patches from low-risk (top) and high-risk (bottom) cases with corresponding cell labels. **F.** Quantification of cell types in high attention patches for all cases of BLCA with high-risk in red and low-risk in blue, showing high tumor cell abundance in both risk groups, with increased stromal cell presence in high-risk groups.

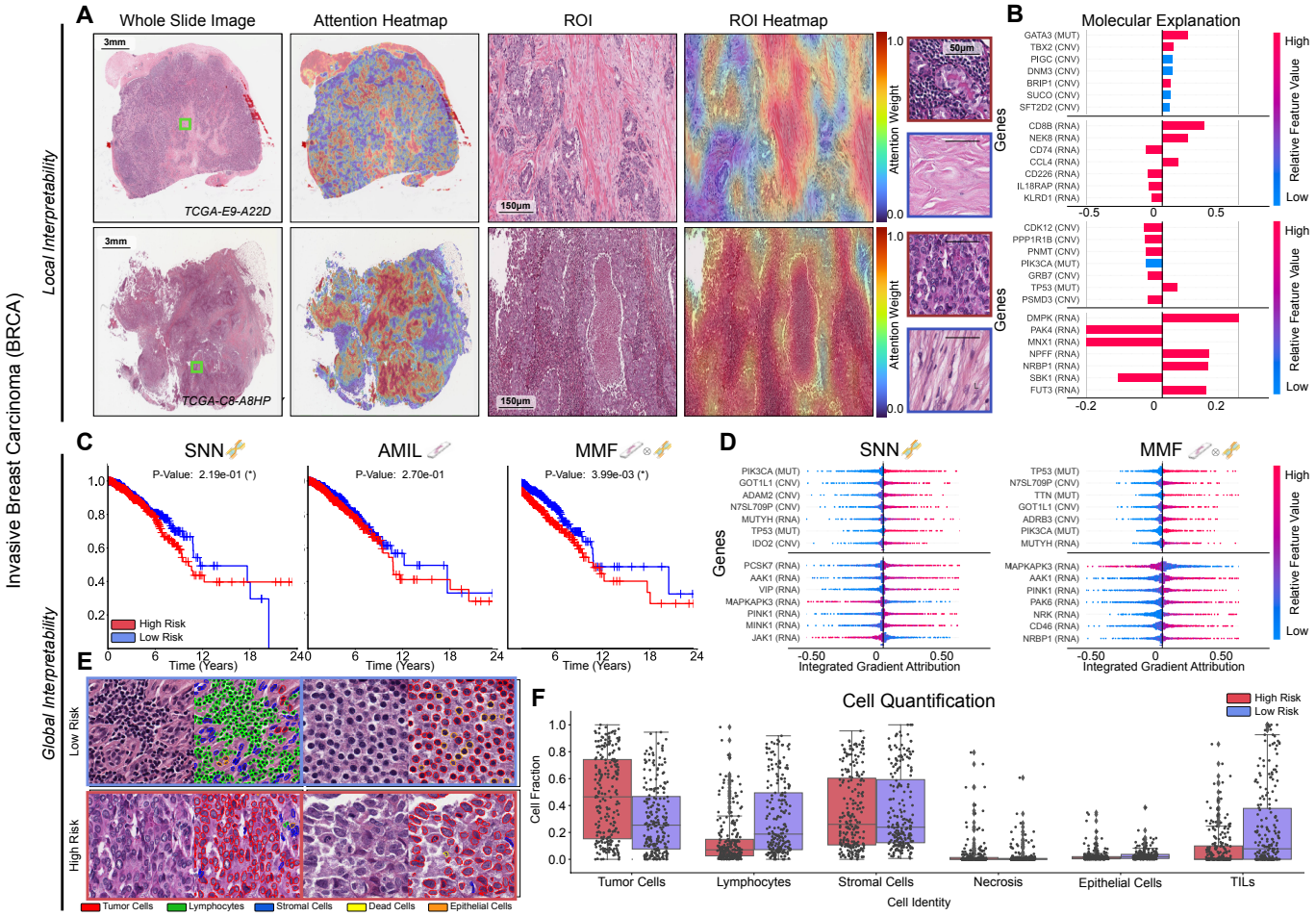

Figure S3: Quantitative performance, local model explanation, and global interpretability analyses of PORPOISE on BRCA. Related to Figure 3, 4, 5, and 6. A. WSIs, associated attention heatmaps, ROIs, ROI heatmaps, and selected high attention patches from example low-risk (top) and high-risk (bottom) cases. In BRCA (n=730), high attention for low-risk cases (n=22) tends to focus on collagenous stroma and aggregates of lymphocytes, while in high-risk cases (n=223), high attention focuses on areas of tumor cells with increased mitotic activity, nuclear pleomorphism, and necrosis. **B.** Local gene attributions for the corresponding low-risk (top) and high-risk (bottom) cases. **C.** Kaplan–Meier curves for omics-only (left, "SNN"), histology-only (center, "AMIL") and multimodal fusion (right, "MMF"), showing improved patient stratification over AMIL and long-surviving patients in SNN. **D.** Global gene attributions across patient cohorts according to unimodal interpretability (left, "SNN"), and multimodal interpretability (right, "MMF"). **E.** High attention patches from low-risk (top) and high-risk (bottom) cases with corresponding cell labels. **F.** Quantification of cell types in high attention patches for each disease overall, showing decreased tumor cell abundance and increased lymphocyte and TIL presence in low-risk groups.

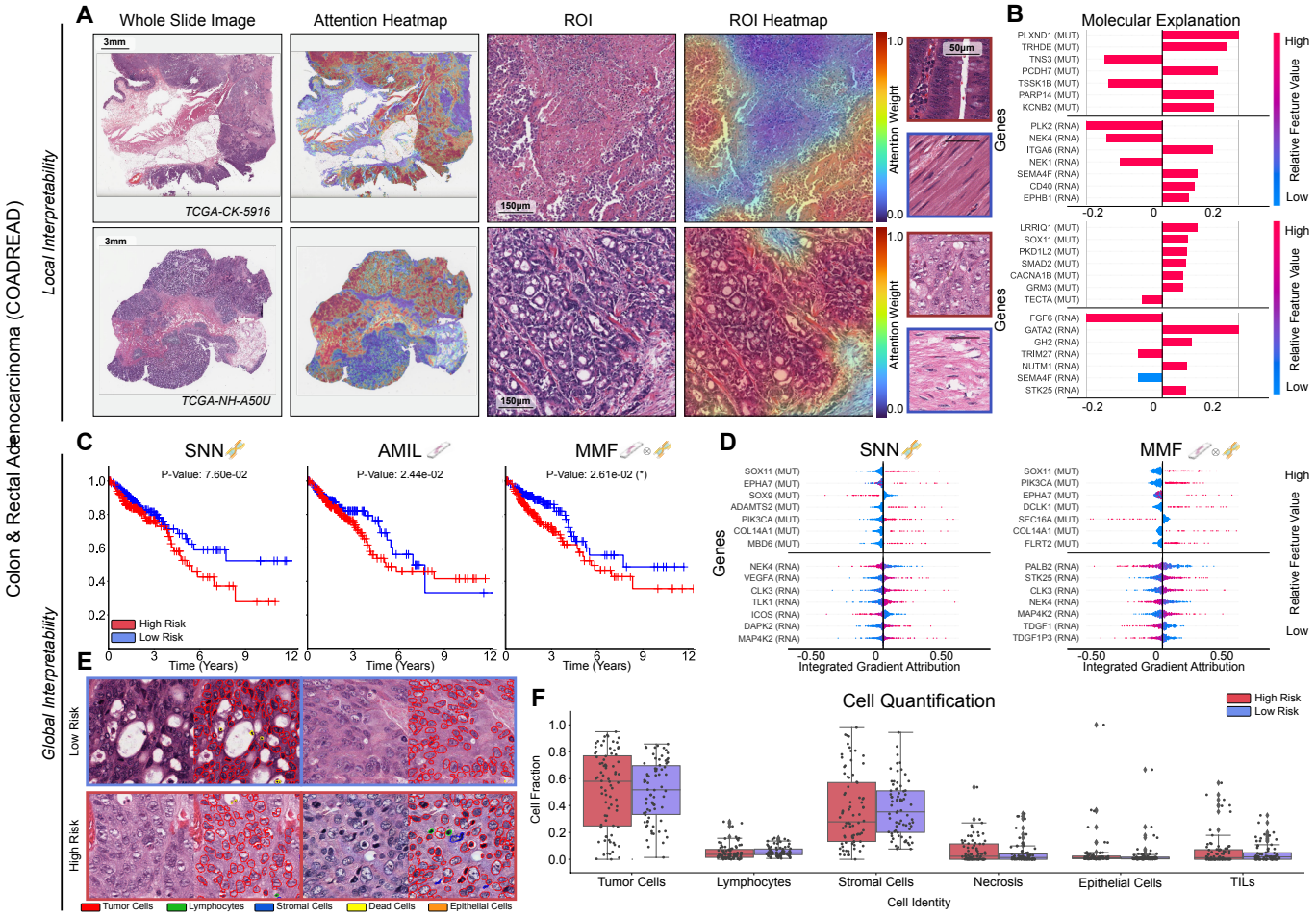

Figure S4: Quantitative performance, local model explanation, and global interpretability analyses of PORPOISE on COADREAD. Related to Figure 3, 4, 5, and 6. A. WSIs, associated attention heatmaps, ROIs, ROI heatmaps, and selected high attention patches from example low-risk (top) and high-risk (bottom) cases. In COADREAD (n=338), high attention for low-risk cases (n=74) tends to focus on muscularis, solid tumor growth and small nests of tumor cells, while in high-risk cases (n=80), high attention focuses on tumor cells invading the submucosa into the musclaris. **B.** Local gene attributions for the corresponding low-risk (top) and high-risk (bottom) cases. **C.** Kaplan–Meier curves for omics-only (left, "SNN"), histology-only (center, "AMIL") and multimodal fusion (right, "MMF"), showing improved patient stratification over AMIL and long-surviving patients in SNN. **D.** Global gene attributions across patient cohorts according to unimodal interpretability (left, "SNN"), and multimodal interpretability (right, "MMF"). **E.** High attention patches from low-risk (top) and high-risk (bottom) cases with corresponding cell labels. **F.** Quantification of cell types in high attention patches for each disease overall, showing similar admixtures of tumor cells, lymphocytes, and stromal cells across both risk groups.

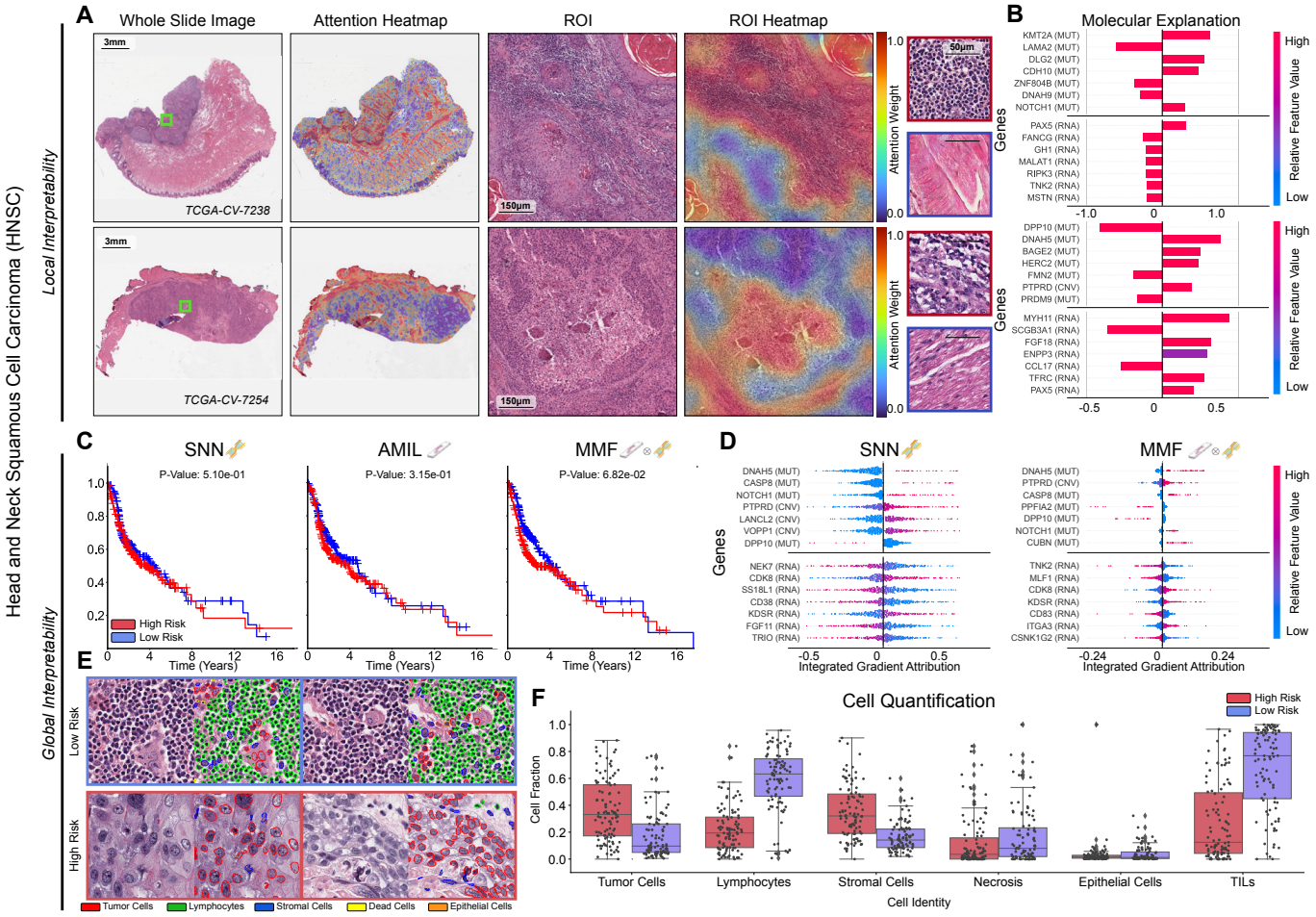

Figure S5: Quantitative performance, local model explanation, and global interpretability pooled analyses of PORPOISE on HNSC. Related to Figure 3, 4, 5, and 6. A. WSIs, associated attention heatmaps, ROIs, ROI heatmaps, and selected high attention patches from example low-risk (top) and high-risk (bottom) cases. In HNSC (n=413), high attention for low-risk cases (n=96) tends to focus on regions with increased tumor infiltrating lymphocytes, while in high-risk cases (n=103), high attention areas corresponded with regions with central necrosis. For both high and low-risk cases, the low attention regions focused on mainly background stroma. **B.** Local gene attributions for the corresponding low-risk (top) and high-risk (bottom) cases. **C.** Kaplan–Meier curves for omics-only (left, "SNN"), histology-only (center, "AMIL") and multimodal fusion (right, "MMF"), with statistically significant patient stratification between low- and high-risk groups across all models. **D.** Global gene attributions across patient cohorts according to unimodal interpretability (left, "SNN"), and multimodal interpretability (right, "MMF"). **E.** High attention patches from low-risk (top) and high-risk (bottom) cases with corresponding cell labels. **F.** Quantification of cell types in high attention patches for each disease overall, showing increased tumor cell presence in the high-risk group, with increased lymphocyte and TIL presence in the low-risk group.

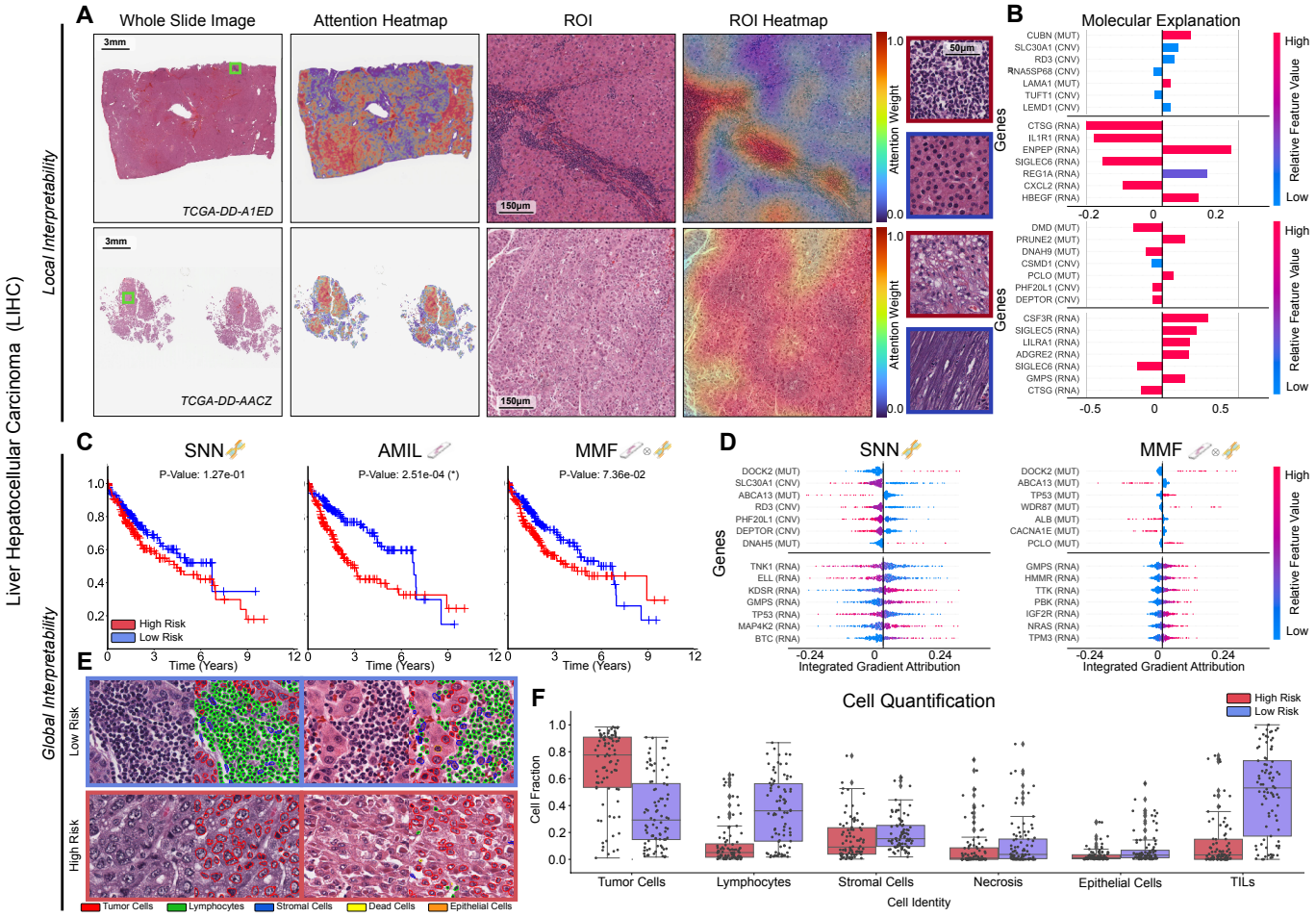

Figure S6: Quantitative performance, local model explanation, and global interpretability pooled analyses of PORPOISE on LIHC. Related to Figure 3, 4, 5, and 6. A. WSIs, associated attention heatmaps, ROIs, ROI heatmaps, and selected high attention patches from example low-risk (top) and high-risk (bottom) cases. In LIHC (n=332), high attention for low-risk cases (n=85) tends to focus on dense regions of lymphocytes, while in high-risk cases (n=84), high attention focuses on areas with high tumor-grade morphology, such as increased nuclear pleomorphism. **B.** Local gene attributions for the corresponding low-risk (top) and high-risk (bottom) cases. **C.** Kaplan–Meier curves for omics-only (left, "SNN"), histology-only (center, "AMIL") and multimodal fusion (right, "MMF"), showing poor stratification with SNN and better stratification in AMIL and MMF. **D.** Global gene attributions across patient cohorts according to unimodal interpretability (left, "SNN"), and multimodal interpretability (right, "MMF"). **E.** High attention patches from low-risk (top) and high-risk (bottom) cases with corresponding cell labels. **F.** Quantification of cell types in high attention patches for each disease overall, showing increased tumor cell presence in high-risk patients and increased lymphocyte and TIL presence in low-risk patients.

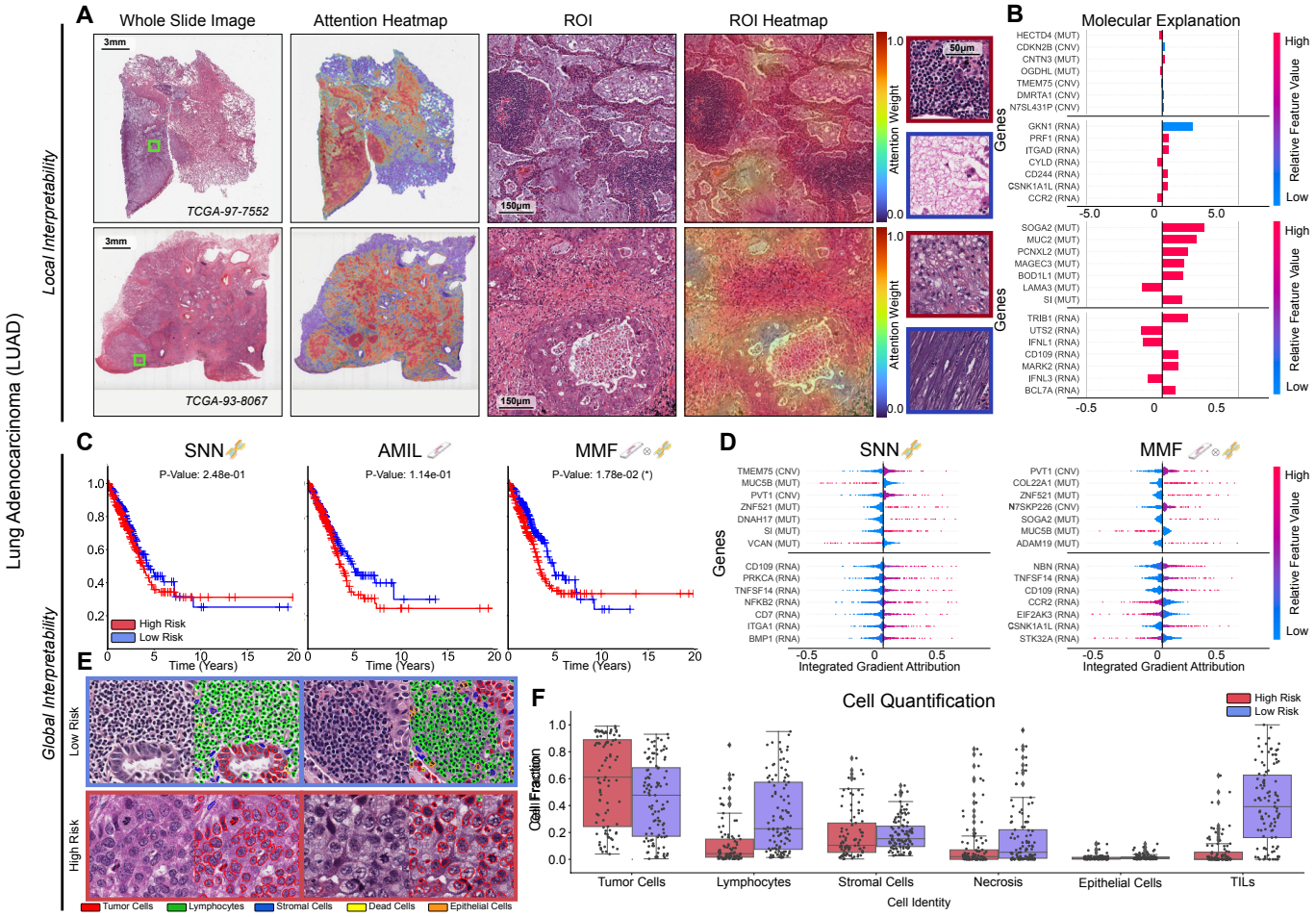

Fig. S7: Quantitative performance, local model explanation, and global interpretability analyses of PORPOISE on LUAD. Related to Figure 3, 4, 5, and 6. A. WSIs, associated attention heatmaps, ROIs, ROI heatmaps, and selected high attention patches from example low-risk (top) and high-risk (bottom) cases. In LUAD (n=431), high attention for low-risk cases (n=105) tends to focus on regions with dense inflammatory infiltrate, predominantly comprised of lymphocytes, and regions of mucin deposition, while in high-risk cases (n=89), high attention focuses on tumor cells with increased nuclear pleomorphism, areas of necrosis, and tumor-associated dense fibrous stroma. **B.** Local gene attributions for the corresponding low-risk (top) and high-risk (bottom) cases. **C.** Kaplan–Meier curves for omics-only (left, "SNN"), histology-only (center, "AMIL") and multimodal fusion (right, "MMF"), showing poor stratification with SNN and better stratification in AMIL and MMF **D.** Global gene attributions across patient cohorts according to unimodal interpretability (left, "SNN"), and multimodal interpretability (right, "MMF"). **E.** High attention patches from low-risk (top) and high-risk (bottom) cases with corresponding cell labels. **F.** Quantification of cell types in high attention patches for each disease overall, showing increased lymphocyte and TIL presence in low-risk patients.

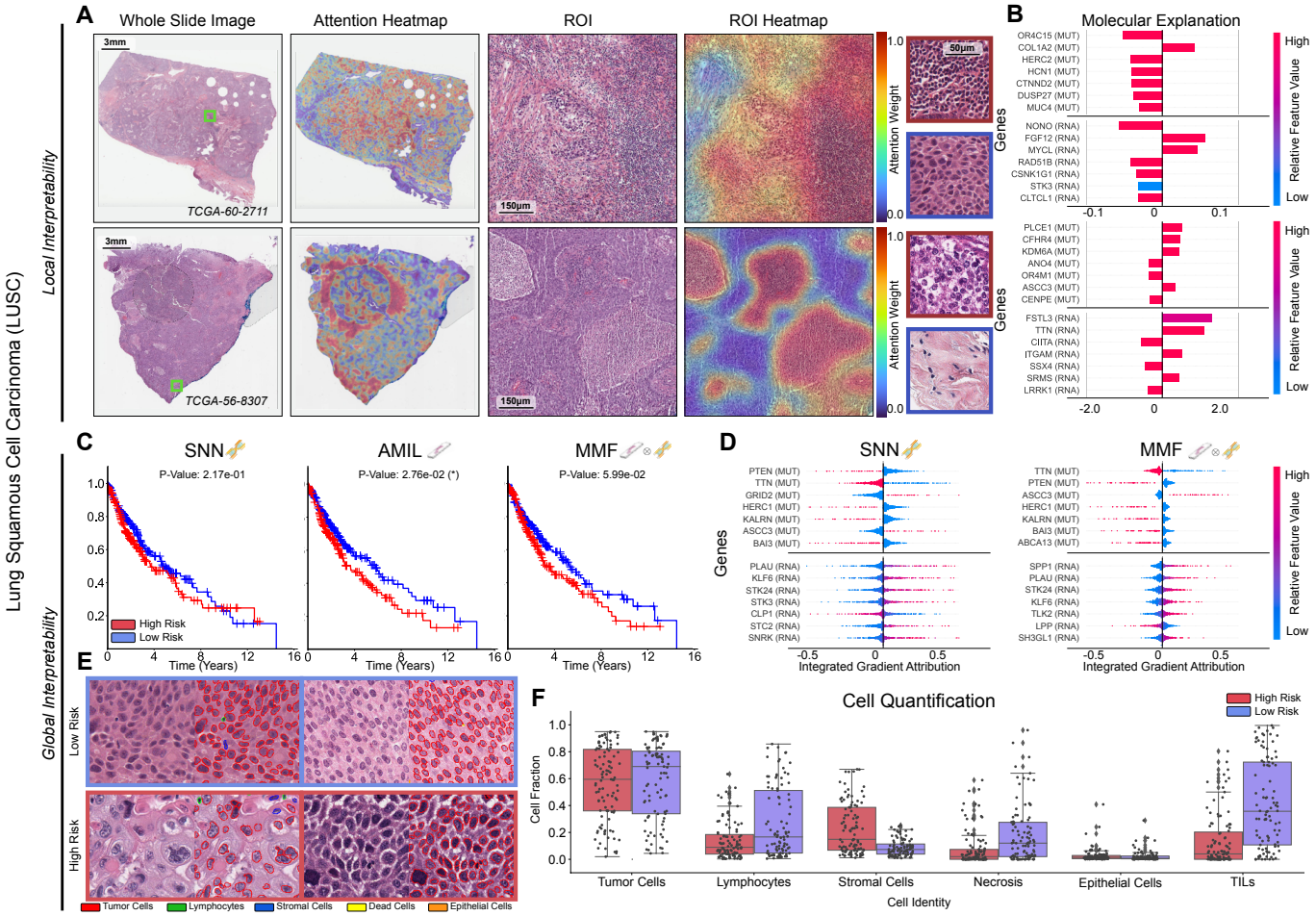

Figure S8: Quantitative performance, local model explanation, and global interpretability pooled analyses of PORPOISE on LUSC. Related to Figure 3, 4, 5, and 6. A. WSIs, associated attention heatmaps, ROIs, ROI heatmaps, and selected high attention patches from example low-risk (top) and high-risk (bottom) cases. In LUSC (n=441), high attention for low-risk cases (n=97) tends to focus on regions with dense inflammatory infiltrate, predominantly comprised of lymphocytes (presumed TILs), while in high-risk cases (n=103), high attention focuses on regions of central necrosis within tumor nests. **B.** Local gene attributions for the corresponding low-risk (top) and high-risk (bottom) cases. **C.** Kaplan–Meier curves for omics-only (left, "SNN"), histology-only (center, "AMIL") and multimodal fusion (right, "MMF"), showing improved patient stratification over AMIL and late-stage patients in SNN. **D.** Global gene attributions across patient cohorts according to unimodal interpretability (left, "SNN"), and multimodal interpretability (right, "MMF"). **E.** High attention patches from low-risk (top) and high-risk (bottom) cases with corresponding cell labels. **F.** Quantification of cell types in high attention patches for each disease overall, showing increased lymphocyte and TIL presence in low-risk patients.

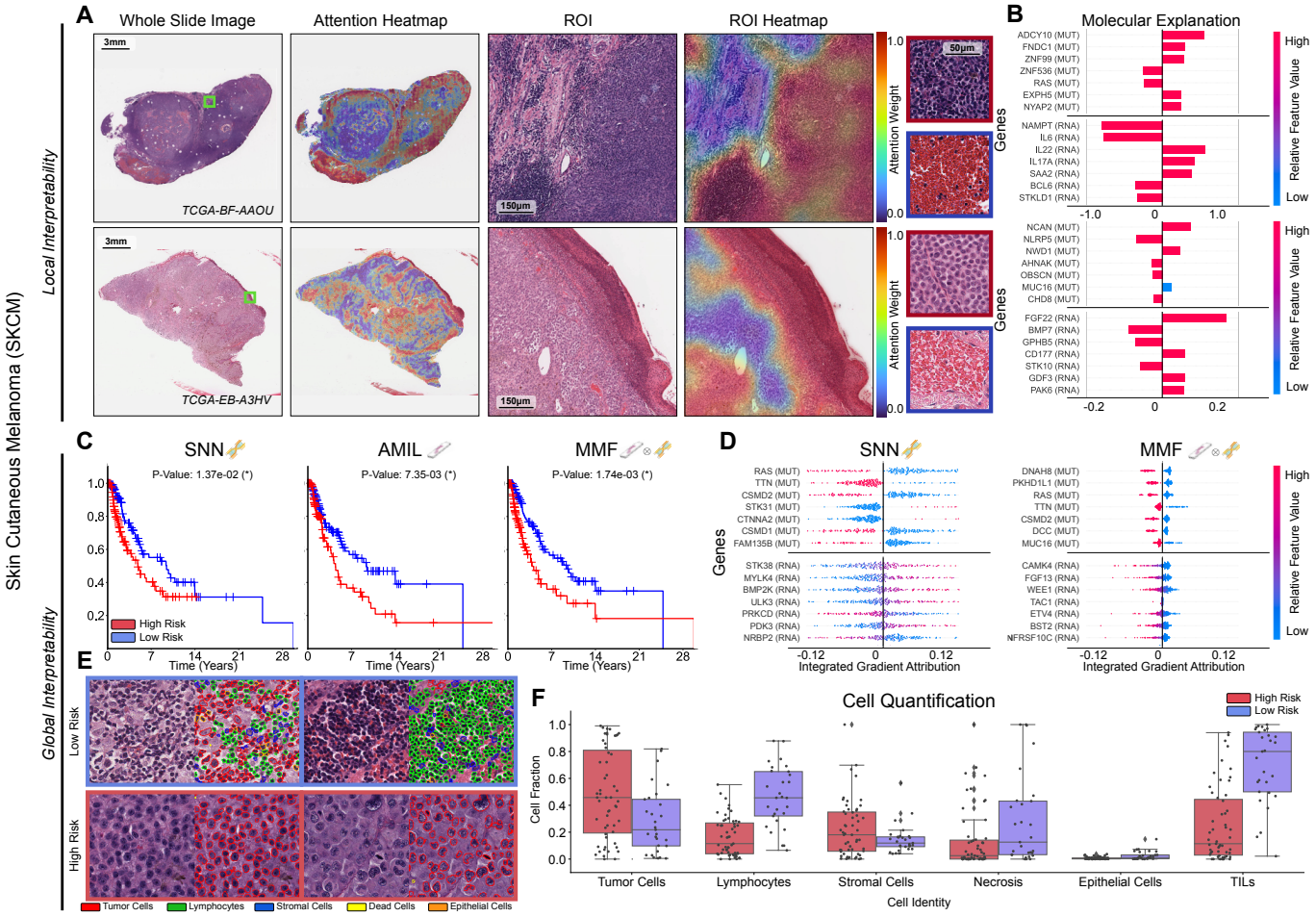

Figure S9: Quantitative performance, local model explanation, and global interpretability pooled analyses of PORPOISE on SKCM. Related to Figure 3, 4, 5, and 6. A. WSIs, associated attention heatmaps, ROIs, ROI heatmaps, and selected high attention patches from example low-risk (top) and high-risk (bottom) cases. In SKCM (n=222), high attention regions for low-risk cases (n=29) focused on tumor-infiltrating lymphocytes, while the high attention regions for high-risk cases (n=55) paid more attention to ulcerated regions and regions of densely packed tumor cells. For both high and low-risk cases, the low attention regions focused mainly on background blood. **B.** Local gene attributions for the corresponding low-risk (top) and high-risk (bottom) cases. **C.** Kaplan–Meier curves for omics-only (left, "SNN"), histology-only (center, "AMIL") and multimodal fusion (right, "MMF"), showing better patient stratification in AMIL and SNN. **D.** Global gene attributions across patient cohorts according to unimodal interpretability (left, "SNN"), and multimodal interpretability (right, "MMF"). **E.** High attention patches from low-risk (top) and high-risk (bottom) cases with corresponding cell labels. **F.** Quantification of cell types in high attention patches for each disease overall, showing increased tumor cell and necrosis presence in the high-risk group, with increased lymphocyte and TIL presence in the low-risk group.

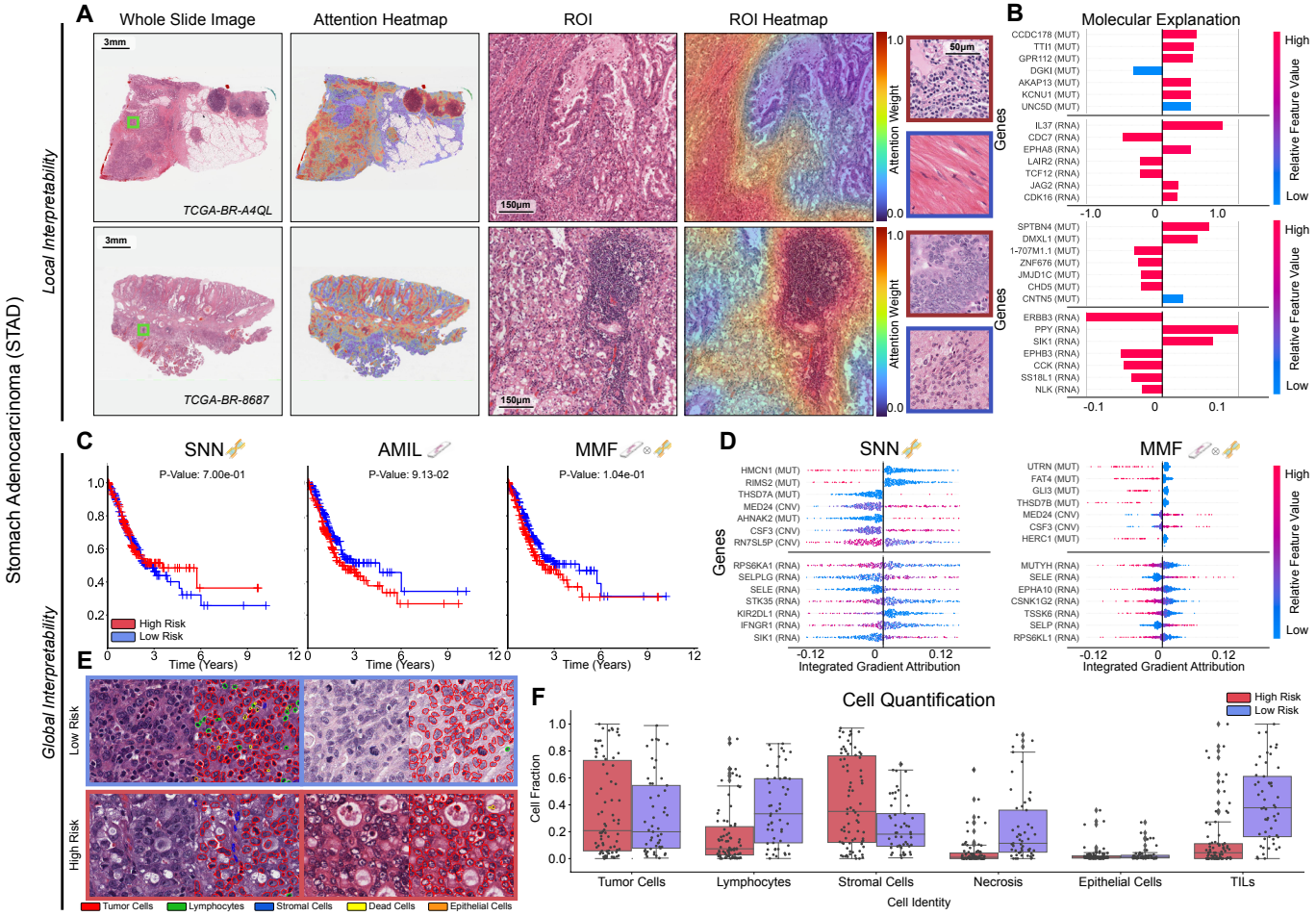

Figure S10: Quantitative performance, local model explanation, and global interpretability pooled analyses of PORPOISE on STAD. Related to Figure 3, 4, 5, and 6. A. WSIs, associated attention heatmaps, ROIs, ROI heatmaps, and selected high attention patches from example low-risk (top) and high-risk (bottom) cases. In STAD (n=347), high attention for low-risk cases (n=53) tends to focus on dense regions of tumor, lymphocytes, and muscularis, while in high-risk cases (n=78), high attention focuses on dense regions of tumor and lymphocytes. **B.** Local gene attributions for the corresponding low-risk (top) and high-risk (bottom) cases. **C.** Kaplan–Meier curves for omics-only (left, "SNN"), histology-only (center, "AMIL") and multimodal fusion (right, "MMF"), showing better patient stratification in AMIL and SNN. **D.** Global gene attributions across patient cohorts according to unimodal interpretability (left, "SNN"), and multimodal interpretability (right, "MMF"). **E.** High attention patches from low-risk (top) and high-risk (bottom) cases with corresponding cell labels. **F.** Quantification of cell types in high attention patches for each disease overall, showing increased lymphocyte and TIL presence in the low-risk group.

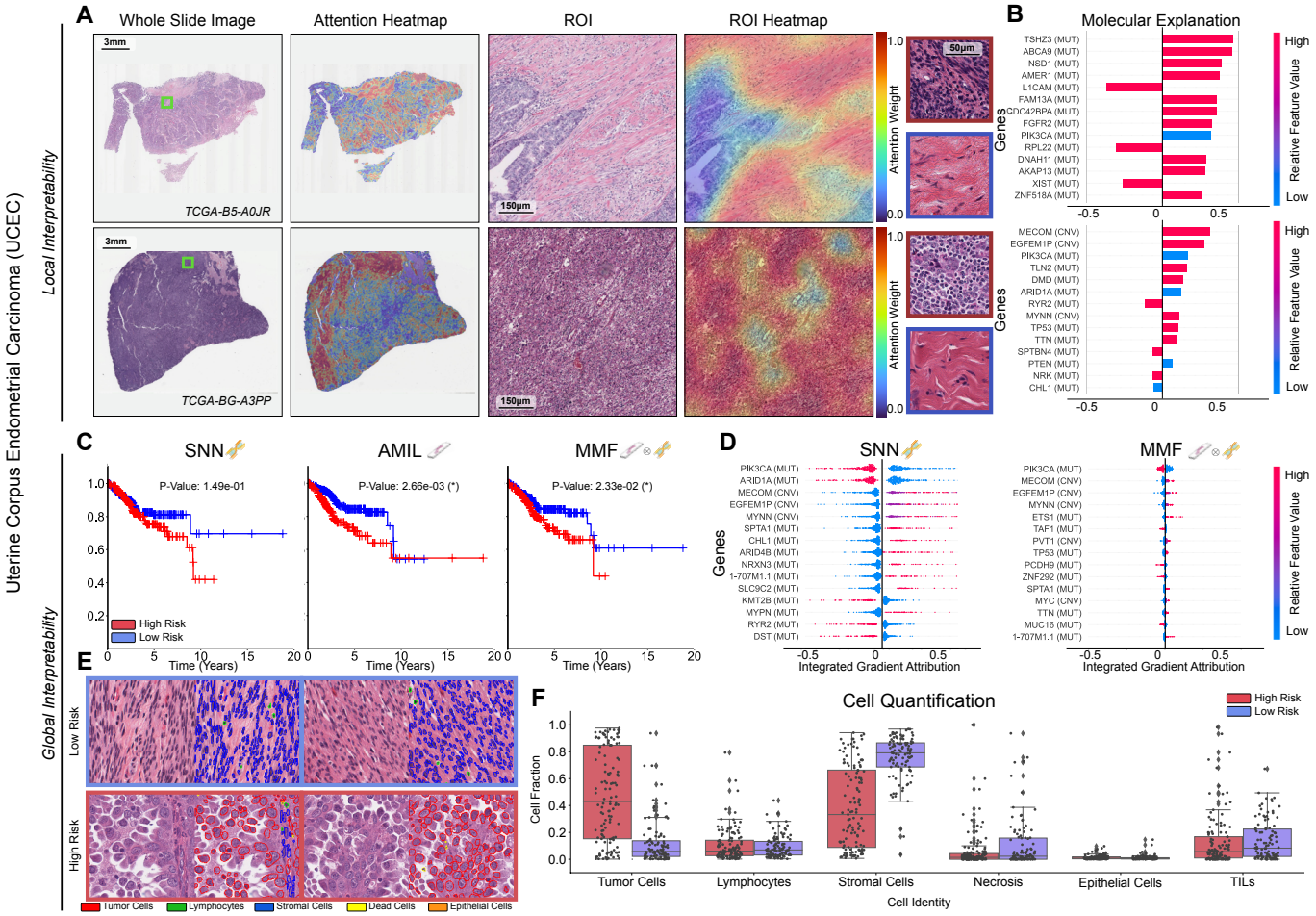

Figure S11: Quantitative performance, local model explanation, and global interpretability pooled analyses of PORPOISE on UCEC. Related to Figure 3, 4, 5, and 6. A. WSIs, associated attention heatmaps, ROIs, ROI heatmaps, and selected high attention patches from example low-risk (top) and high-risk (bottom) cases. In UCEC (n=460), high attention for low-risk cases (n-104) tends to focus on background myometrium, while in high-risk cases (n=125), high attention focuses on tumor regions, especially those with increased nuclear pleomorphism and atypia. **B.** Local gene attributions for the corresponding low-risk (top) and high-risk (bottom) cases. **C.** Kaplan–Meier curves for omics-only (left, "SNN"), histology-only (center, "AMIL") and multimodal fusion (right, "MMF"), showing improved patient stratification over AMIL and late-stage patients in SNN. **D.** Global gene attributions across patient cohorts according to unimodal interpretability (left, "SNN"), and multimodal interpretability (right, "MMF"). **E.** High attention patches from low-risk (top) and high-risk (bottom) cases with corresponding cell labels. **F.** Quantification of cell types in high attention patches for each disease overall, showing increased tumor cell presence in high-risk patients and increased stromal cell presence in low-risk patients.

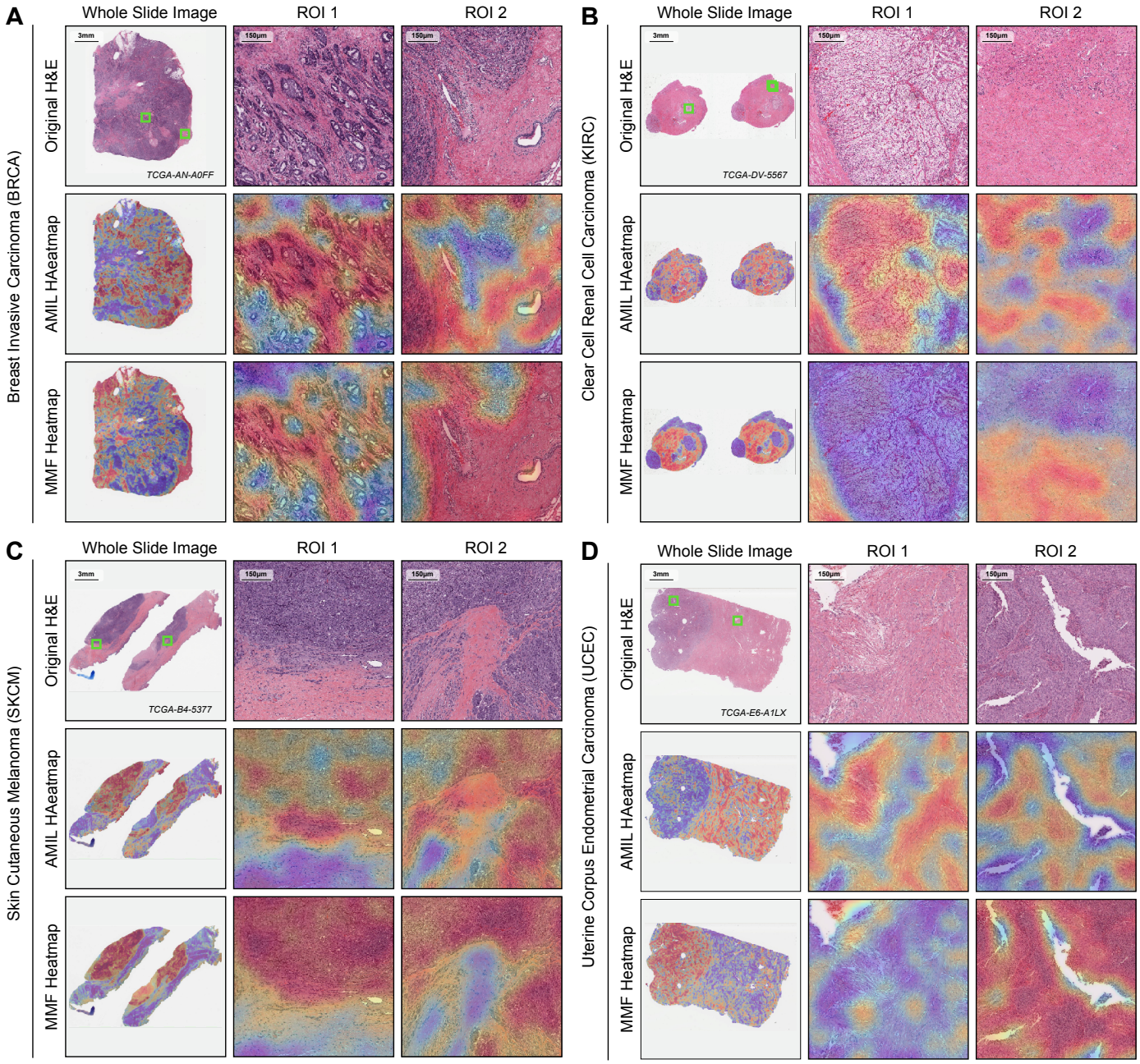

Figure S12: Exemplars of attention shift from unimodal to multimodal interpretability in WSIs. Related to Figure 2. Using PORPOISE, we investigated and examined how feature importance in high attention regions shifts when comparing AMIL (trained with histology-only) vs. MMF (histology conditioned with molecular profiles). In the assessment of each cancer type, "ROI 1" corresponds to a region where attention decreased from AMIL to MMF, and "ROI 2" corresponds to a region where attention increased from AMIL to MMF. **A.** In BRCA, attention shifted away from dense areas of tumor to both tumor and stromal regions in MMF. **B.** In KIRC, both stroma and tumor regions with classic "chicken-wire" vasculature are present in high attention regions in AMIL, whereas MMF attends to only stroma and completely segments out the tumor regions. **C.** In SKCM, both AMIL and MMF were able to localize tumor regions, with MMF being able to identify clear tumor-stroma boundaries. **D.** In UCEC, attention shifted towards dense tumor regions and away from stroma in MMF.

Supplemental Tables

Table S1. TCGA Pan-Cancer Demographic Characteristics. Related to Figure 1 and 2.

Cancer	No. Cases	Age	Gender M/F	White/Black/Other/NA	Grade 1/2/3/4/NA	Censorship
BLCA	373	68.0 ± 10.6	277/96	297/20/42/0/14	20/0/0/351/2	0.547
BRCA	730	57.4 ± 13.3	10/720	490/138/43/1/62	NA	0.860
COADREAD	339	64.9 ± 13.0	180/159	247/56/12/1/27	NA	0.761
HNSC	416	61.2 ± 11.9	307/109	353/42/8/2/13	53/247/100/4/12	0.526
KIRC	345	60.1 ± 12.0	219/126	283/50/7/0/6	11/146/135/46/7	0.733
KIRP	259	61.5 ± 12.1	189/70	183/58/6/1/12	NA	0.846
LGG	479	43.4 ± 13.4	268/211	453/21/7/1/10	0/229/249/0/1	0.766
LIHC	333	59.3 ± 13.2	223/110	165/13/149/0/8	44/160/112/12/5	0.655
LUAD	453	65.2 ± 10.0	208/245	344/51/7/1/52	NA	0.651
LUSC	450	67.2 ± 8.6	336/114	315/27/9/0/99	NA	0.573
PAAD	166	64.5 ± 11.0	91/75	146/6/11/0/4	26/91/45/2/2	0.458
SKCM	230	59.5 ± 15.6	140/90	220/1/9/0/6	NA	0.613
STAD	348	65.3 ± 10.5	227/121	211/10/80/1/46	8/123/209/0/8	0.601
UCEC	480	63.9 ± 11.1	0/480	326/96/19/11/29	94/113/265/8	0.844

Table S2. c-Index Model Performances on Survival Prediction across 14 Cancer Types with Logrank Test Significance for Patient Stratification. Related to Figure 2.

Study	SNN	P-Value	MIL	P-Value	MMF	P-Value
BLCA	0.595 (0.535-0.637)	2.35e-03	0.542 (0.486-0.580)	2.14e-01	**0.631 (0.572-0.671)**	2.30e-03
BRCA	0.586 (0.525-0.643)	2.19e-01	0.560 (0.489-0.615)	2.70e-01	**0.628 (0.571-0.680)**	3.99e-03
COADREAD	0.580 (0.496-0.654)	7.60e-02	0.546 (0.466-0.617)	2.44e-01	**0.640 (0.562-0.705)**	2.61e-02
HNSC	0.516 (0.478-0.572)	5.10e-01	0.564 (0.507-0.592)	3.15e-01	**0.573 (0.525-0.617)**	6.82e-02
KIRC	0.633 (0.567-0.697)	2.99e-02	0.567 (0.508-0.650)	5.98e-02	**0.659 (0.589-0.709)**	4.38e-06
KIRP	0.779 (0.678-0.857)	2.27e-03	0.539 (0.408-0.625)	5.86e-01	**0.816 (0.705-0.880)**	3.83e-04
LGG	0.792 (0.738-0.841)	5.68e-10	0.668 (0.614-0.734)	1.82e-04	**0.808 (0.745-0.844)**	7.09e-12
LIHC	0.594 (0.534-0.656)	1.27e-01	0.618 (0.563-0.684)	2.51e-04	**0.622 (0.559-0.681)**	7.36e-02
LUAD	0.554 (0.493-0.613)	2.48e-01	0.548 (0.489-0.597)	1.14e-01	**0.600 (0.548-0.657)**	1.78e-02
LUSC	0.522 (0.476-0.572)	2.17e-01	**0.561 (0.500-0.597)**	2.76e-02	0.538 (0.472-0.575)	5.99e-02
PAAD	0.593 (0.507-0.656)	5.59e-02	0.580 (0.485-0.613)	2.30e-01	**0.653 (0.571-0.696)**	1.69e-03
SKCM	0.644 (0.568-0.691)	1.37e-02	0.607 (0.509-0.661)	7.35e-03	**0.651 (0.581-0.710)**	1.74e-03
STAD	0.513 (0.453-0.560)	7.00e-01	0.556 (0.494-0.598)	9.13e-02	**0.563 (0.496-0.607)**	1.04e-01
UCEC	0.580 (0.484-0.621)	1.49e-01	**0.638 (0.563-0.701)**	2.66e-03	0.634 (0.527-0.667)	2.33e-02
Overall	0.606	-	0.578	-	**0.644**	-